Journal of Ambient Intelligence and Humanized Computing
https://doi.org/10.1007/s12652-018-1051-5

ORIGINAL RESEARCH

Skin lesion segmentation and recognition using multichannel saliency estimation and M-SVM on selected serially fused features

Tallha Akram[1] · Muhammad Attique Khan[2] · Muhammad Sharif[3] · Mussarat Yasmin[3]

Received: 10 March 2018 / Accepted: 15 September 2018
© Springer-Verlag GmbH Germany, part of Springer Nature 2018

Abstract
The number of deaths caused by melanoma has increased remarkably in the last few years which are the carcinogenic type of skin cancer. Lately, computer based methods are introduced which are intelligent enough to support dermatologist in initial judgment of skin lesion. However, there still exists a gap for an optimal solution; therefore, machine learning community is still considering it a great challenge. The primary objective of this article is to efficiently detect and classify skin lesion with the utilization of an improved segmentation and feature selection criteria. Presented contribution is threefold; First, ternary color spaces are exploited to separate foreground from the background—utilizing multilevel approach of contrast stretching. Second, a weighting criterion is designed which is able to select the best solution based on extended texture feature analysis, related labels, boundary connections and central distance. Third, an improved feature extraction and dimensionality reduction criteria is proposed which combines conventional as well as recent feature extraction techniques. The proposed method is tested on PH2, ISBI 2016 and ISIC benchmark data sets and evaluated on the basis of multiple parameters including FPR, sensitivity, specificity, FNR and accuracy. From the statistics, it is quite clear that the proposed method outperforms numerous existing techniques with considerable margin.

Keywords Skin cancer · Image enhancement · Image fusion · Feature extraction · Feature selection

1 Introduction

Melanoma is one of the deadliest types of cancers responsible for massive number of deaths worldwide (Codella et al. 2018; Oliveira et al. 2018). Although it accounts for approximately 3–4% of all skin cancer cases, still it is the primary source of death of around 75% people related to skin cancers (Codella et al. 2018). In America alone, 178,560 melanoma cases are reported in 2018 including 91,270 invasive and 87,290 non invasive cases. Whereas the estimated total deaths in 2018 are 9320 containing 3330 women and 5990 men (Siegel et al. 2018). In Australia, an estimated number of skin cancer cases treated in 2018 are 14,320 including 8653 males and 5667 females. Estimated number of deaths in 2018 due to skin cancer are 1905 including 1331 males and 574 females (Read et al. 2018).

Discriminating benign (a common nevi) and melanoma (a lethal skin cancer) at their early stages is quite difficult as they both exhibit similar features at early evolutional phase which is one of the main problems for an expert dermatologist. The primary reasons behind are morphological structural factors of lesion like color spectrum, shades of color lesion skin gradient, multiple lesions, streaks and grid patterns (Hendi and Martinez 2011). Figure 1 shows skin lesion images taken from two different data sets. The severity of pigmented skin cancer and its resulting demise can be curtailed if it is detected at an early step of inception. Melanoma is almost curable and survival rate increases if it is detected when the malignanttumor thickness is less than a specific threshold and at its very early stage (Brunssen et al. 2017; Sng et al. 2009).

In clinical interpretation, the doctors utilize dermoscopy for lesion detection. Dermoscopy is a non invasive method used to study the skin lesion in dermatology. In clinical examination, the most commonly visual inspection methods are ABCD rule (Kawahara et al. 2018; Monisha et al. 2018),

✉ Mussarat Yasmin
mussaratabdullah@gmail.com

[1] Department of Electrical Engineering, COMSATS University Islamabad, Wah Campus, Wah Cantt, Pakistan

[2] Department of Compute Science and Engineering, HITEC Univesity, Museum Road, Taxila, Pakistan

[3] Department of Computer Science, COMSATS University Islamabad, Wah Campus, Wah Cantt, Pakistan

Published online: 24 September 2018

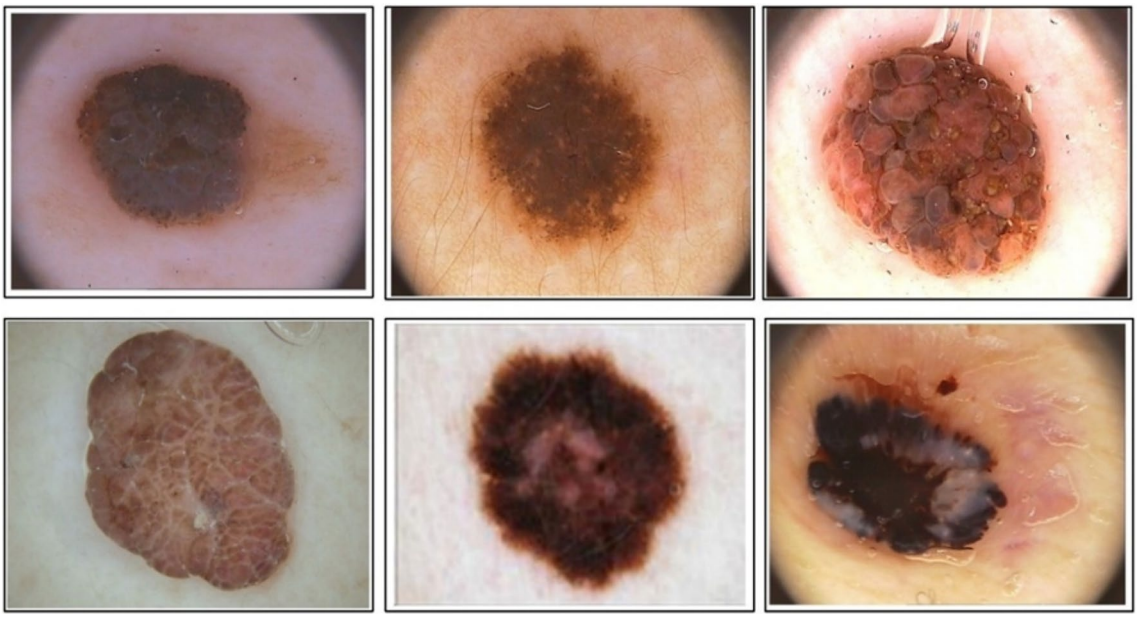

Fig. 1 Samples skin lesion images. First row: images from PH2 data set; second row: images from ISBI 2016 data set

Menzies method (Johr 2002), 7-point check list(Johr 2002) and several other optical techniques. The clinical methods have sufficient possibilities to determine the skin lesions and to accurately identify melanoma and benign. In clinical tests, optical methods are mostly utilized to assess the presurgical borders of basal cell carcinoma (Dhane et al. 2016, 2017; Gambichler et al. 2011). Therefore, to achieve high success rate in melanoma diagnosis, several computer based methods are introduced to deal with this problem (Barata et al. 2014). The computeraided diagnosis (CAD) is a much more useful tool for both dermatologists and non-dermatologists for the detection of lesion part in the image (Ansari and Sarode 2017). A computer vision system in this domain has enough potential and has high success rate in facilitating the dermatologist for an early detection of melanoma (Pennisi et al. 2016). Such automated system relies mostly on multiple but fundamental steps including data acquisition of skin (dermoscopic images), contrast enhancement, lesion extraction, feature extraction and finally classification (Bokhari et al. 2018).

1.1 Motivation and problem statement

Computer vision (CV) is an inter disciplinary field that efficiently deals with the range of inputs (images, electric signals, etc.) from some external sources and processes them to generate effective output making the interpretation easy for humans. The primary benefits of utilizing such intelligent systems are accurate interpretations for almost all types of signals in the electromagnetic spectrum from gamma to radio waves. On the other hand, human eye is limited to the visible light band spectrum only. Almost all domains under the umbrella of CV require processing of input images to perform some actions. This processing is done in various steps including preprocessing, segmentation, feature extractionto name a few. Specifically, in the field of medical imaging, segmentation and classification of skin lesion gained much attention recently. For this purpose, systems were developed (Khan et al. 2018a, b; Shereena and David 2014), amongst them majority are following series of inter connected steps which start from contrast improving and end at classification. These advanced machine learning methods not only help doctors for accurate detections but also learning fast and are on the verge of taking precise decisions. Artificial intelligence is now getting more insight into our lives as decisions in several places are taken by the machines due to a breakthrough in machine learning. This is a fact that researchers are covering different real domains while nourishing them with advanced machine learning techniques.In preprocessing step, several noise factors are tackled including skin artifacts removal such as low contrast and thick hairs. In the segmentation step, lesion regions are detected automatically which is a crucial task due to several problems such as lesion shape, irregularity, asymmetry, and color and border area. This step is also important and plays its vital role in feature extraction stage with the fact that accurate features produce best classification results.The purpose of all this processing is to classify skin lesion to provide information about the extent of disease and helps to plan treatment.

1.2 Contributions

Recently, most of the approaches emerged in this field are features dependent which are later classified using range of algorithms. Feature are basically extracted using two different methods; (1) using rules proposed by medical experts called ABCD rules; (2) features directly calculated from the images including texture, shape and color. In this article, primary focus is to segment lesion by utilizing features from both medical experts and directly CV techniques. The primary contributions are:

Ternary color spaces including CIE-Lab, CIE-YCbCr and CIE-LUV are exploited to identify most relevant channel. A weighting criterion is also proposed which extracts the most appropriate channel having maximum saliency information. A fusion mechanism is also proposed on features calculated from both ways mentioned earlier to secure maximal information. An addition of dimensionality reduction using neighborhood component analysis (NCA) avoids feature correlation and redundancy.

2 Background

Early detection generates a chance for the dermatologist to decrease the rate of skin lesion for humans. Recently, due to advancement in the domain of computer vision, several computer based methods are introduced (Al-Ayyoub et al. 2018; Eltoukhy et al. 2018; Khan et al. 2018a; Nasir et al. 2018). Most of the works in this domain have focused on conventional approaches which used low-level and mid-level features with conventional machine learning algorithms (Capdehourat et al. 2011). In medical imaging, contrast enhancement is a serious issue which affects the segmentation and feature extraction process. Sri et al. (Raja et al. 2018) introduced an enhancement method for MRI images to explore the location and severity of disease. For this purpose, a semi-automated tool is used which improves the contrast of T1 modality.

Recently, several methods solve the classification problem even under challenging conditions such as variability in the appearance of skin lesions (Monisha et al. 2018). Ferris et al. (2015) introduced a decision based approach for skin lesions classification. In feature extraction step, they calculated 54 features and then utilized Decision Forest Classifier (DFC). The experimental results were evaluated on 198 images including 93 benign and 105 melanomas and showed improved performance. Machado et al. (2015) presented a lesions classification method using Gray Level Co-occurrence Matrix (GLCM) and Laws Energy Masks (LEM) features which were later classified by an Ada-Boost algorithm. Similarly, Arroyo and Zapirain (2014) designed a pigmented network for melanoma detection from dermoscopic images. The designed framework consists of two steps, (1) constructing a mask with pixel candidates using machine learning method; (2) searching the desired pigmented network. For this purpose, color and spectral features were extracted. The designed system was evaluated on 220 dermoscopic images and achieved sensitivity of 86% and specificity of 81.67%.

Capdehourat et al. (2011) utilized a classical method to remove the artifacts (hairs) and then lesion region was segmented using color based Otsu method. Thereafter, global and local features were extracted classified by an Ada-Boost algorithm with C4.5 decision trees learning method. The introduced method was tested on a total of 655 dermoscopic images including 544 benign and 111 melanomas and achieved sensitivity above 90%. Premaladha and Ravichandran (2016) introduced a CAD system which consists of four primary steps. In the first step, contrast stretching was performed using Contrast Limited Adaptive Histogram Equalization (CLAHE) and median filter. Second step segmented the lesion region using a new normalized Otsu method which worked efficiently for inconstant illumination. Afterwards, several features such as GLCM, principal component analysis (PCA) and Fourier packet transform (FPT) were extracted. Finally, the features were classified with the fusion of ada-boost and support vector machine (SVM) algorithms. Dalila et al. (2017) introduced a biologically inspired computing (Ant Colony) based segmentation method for skin lesion detection. Three different types of features such as geometric, color and texture were extracted and fed into artificial neural network (ANN) and K nearest neighbor (KNN) classifiers for classification. Total 172 dermoscopic images were used including 88 melanomas and 84 benign for system evaluation. The results reveal that ANN gives promising results as compared to KNN.

Most of the computer based methods work on shape features, color features, texture features, geometric features and multiple classifiers as ANN, SVM, Ada-Boost and KNN are utilized to produce the promising results. Moreover, it is also observed that the conventional approaches for skin lesion classification are highly dependent on the selection of best features. Additionally, optimal features selection methods showed much improvement lately in terms of accuracy in medical imaging (Kushwaha and Pant 2018; Li et al. 2018). Recently, Wu et al. (2018) presented a features selection method based on mutual information (MI) along with entropy concept. The features having maximum MI with ground truth are selected for final classification. Prabukumar et al. (2017) introduced a Cuckoo search algorithm for optimal feature extraction.

This article addresses two primary steps to make the proposed system more efficient: (a) lesion segmentation, and (b) extraction and selection of most robust features.

3 Proposed approach

In dermoscopic images, classification is still a greater challenge which is efficiently dealt with the proposed approach. The core architecture is comprised of multiple steps including preprocessing, foreground segmentation, feature extraction and labeling/ classification, as shown in Fig. 2. In the preprocessing step, hair removal is done because their presence in an image causes noisy segmentation. In the segmentation step, a method is formulated to detect the infected regions. Next step is feature extraction where 7 different features are amalgamated. Finally, classification is performed based on multiple state-of-the-art classifiers.

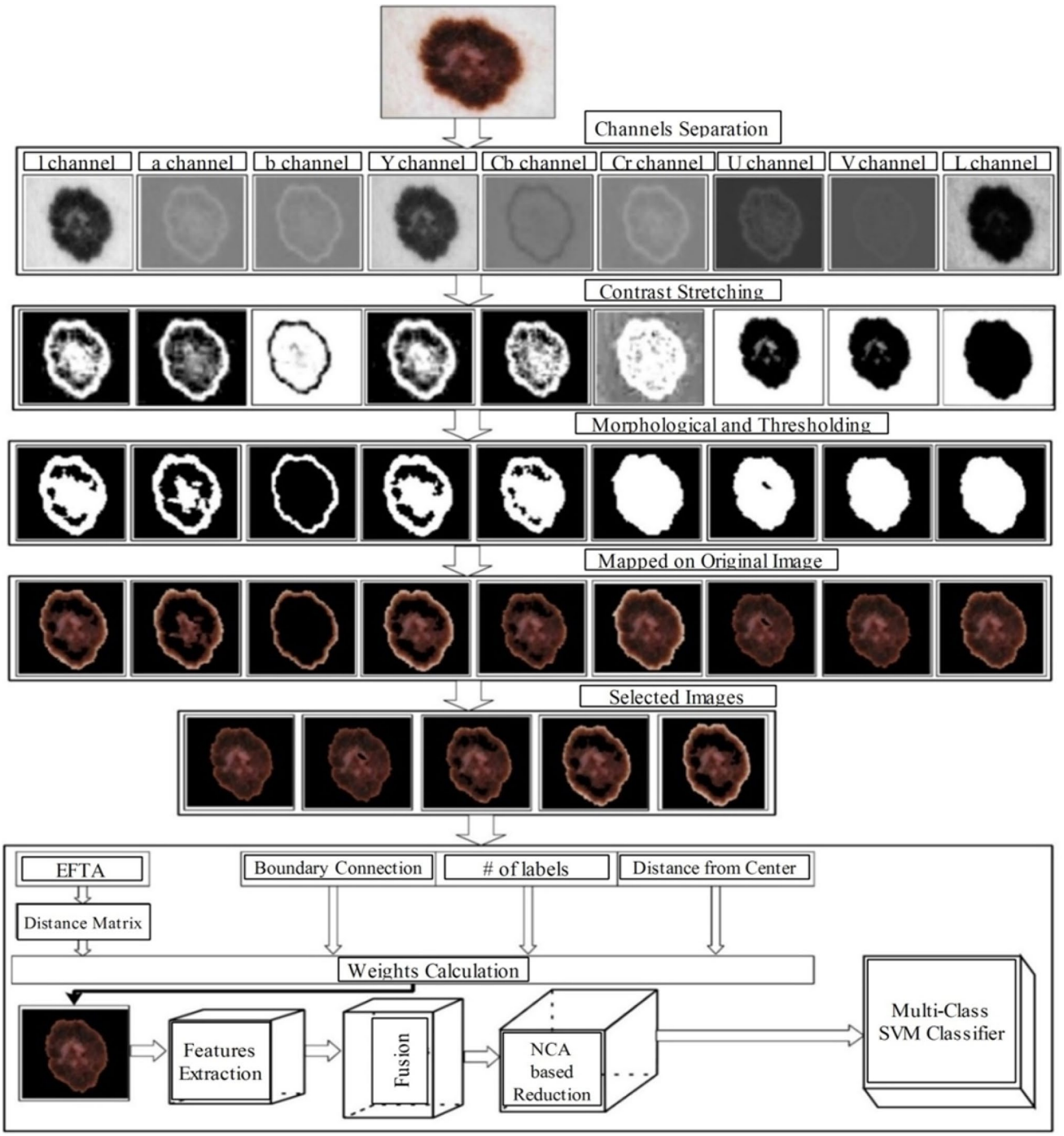

Fig. 2 Proposed flow diagram of skin lesion detection and classification

3.1 Preprocessing

After the acquisition of dermoscopic image several times, the acquired image does not fulfill the basic criteria before subjecting to the next step of image segmentation; therefore it is quite important to preprocess it before further utilization. The preprocessing step tackles the imperfections incorporated in the image at its initial step of acquisition and eliminates multiple artifacts such as hair or ruler markings. The main reason is that their presence usually causes noisy segmentation. Thus, an application to remove hairs and recover the occluded area under hairs is unavoidable. Ideally, image should be acquired after hair exclusion such as by razor shave. However, due to inconvenience in shaving hair before image acquisition, an algorithmic approach to remove hairs is followed. In this work, an automatic well known software Dull Razor (Okuboyejo et al. 2013) is used. This software identifies the hair segments and lines those are in painted by interpolating the most lesion or skin image pixels.

3.2 Saliency segmentation approach

In this section, an efficient segmentation technique is developed for dermoscopic images based on salient region detection. Keeping in view the previous research, basic properties of salient regions (Aksac et al. 2017) can be easily visualized as follows:

1. A salient region demonstrates distinct color and contrast features when compared with the surrounding background.
2. A salient region has distinctive orientation and textural details as compared to the background.
3. A salient region exhibits a uniform color distribution. This means that overall parts of a salient object are homogeneously highlighted.

Mostly RGB dermoscopic images available contents respect the characteristics of salient region; this can also be shown in every color space.

3.2.1 Choice of color space

In salient region detection, a unique approach of considering multiple channels of different color spaces is opted with the gist of finding regions of interest. The first problem is to choice for an appropriate color space having close match to human perception. Color space is a way of representing color information based on certain criteria and is generally divided in four types (Busin et al. 2008). The primary reason behind selecting luminance chrominance channel is the separation of luminance from chroma (light and color in distinct color channels). As proposed algorithm is considering each color channel as an independent gray image, therefore with this separation, the chances of capturing required area increases as compared to three channels combined. Luminance chrominance color spaces efficiently detach both light and color components when comparing with other spaces like RGB or XYZ. Mathematically, the luminance channel is extracted from LAB color spaces and computed as follows in Eq. (1) and Eq. (2):

$$L = 116(F(t) - 16) \tag{1}$$

$$F(t) = \begin{cases} t^{\frac{1}{3}} & t > (6/29)^3 \\ \frac{1}{3}(4.83)^2 t + 0.137 & Otherwise \end{cases} \tag{2}$$

The selected luminance channel is shown in Fig. 3. Due to better visual representation, in the proposed method, luminance chrominance color space is selected and an interesting fact is observed that the salient regions reveal themselves in one or more channels in three selected color spaces (CIE-Lab, CIE- YC_bC_r and HSV).

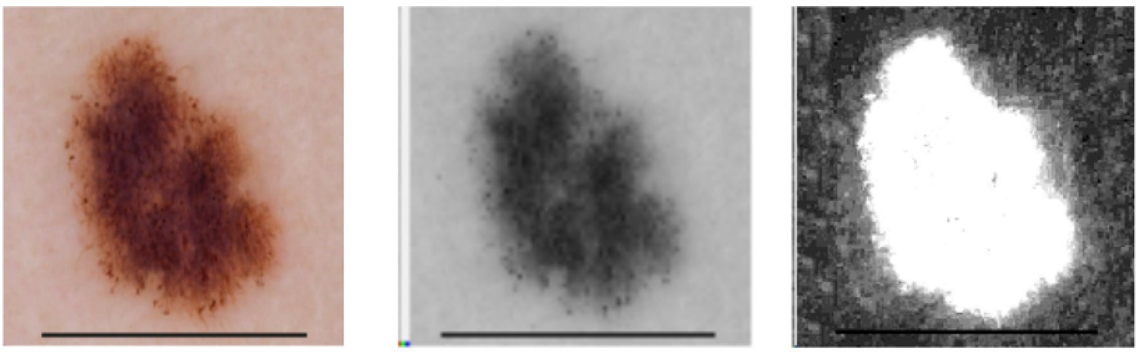

(a) (b) (c)

Fig. 3 Selected luminance channel with contrast stretching affects. **a** Original RGB image, **b** selected luminance channel, and **c** contrast stretching on selected channel

3.2.2 Contrast stretching

In the second step, contrast stretching is applied which is also called normalization. It is an image stretching technique which improves image quality by modifying the range of intensity values (Ravindraiah 2012). Numerous techniques of contrast stretching technique have been proposed in the literature and most of them pick gray image for further processing (Kaur et al. 2011). In the presented approach, all selected channels are enhanced with dimensions (m × n × 1) of selected color spaces having dimensions (m × n × 3).

The provided dermoscopic images (PH2, ISIC, ISBI 2016 datasets) respect the most fundamental assumption that contrast apparentness between lesion and background is high (fulfilling the general properties of salient region). The general properties of saliency/salient foreground and background regions should have color/textural differences. Proposed method is following the same trend; therefore, the selected data sets are subsequent on this assumption and are applicable only on these skin tones. In case of Asians/African skin tone, if foreground and background are having visual differences then salient or infected regions will be identified. Otherwise, algorithm will not be giving improved results. Several approaches utilize background prior and boundary prior (Zhang et al. 2017; Zhu et al. 2014) in order to improve salient region detection. In this work, the image is divided into blocks of equal size and then weights of all regions are calculated for each channel. The detailed architecture of information histogram is explained below:

1. Initially, the dermoscopic image is transformed using sobel edgefilter prior to gradient computation keeping kernel size of 3 × 3.
2. Splitting the gray image and rearranging with respect to gradient intensities by following the ascending order and into multiple blocks (4, 8, 12, …) of equal size. Now for each block, weights are adjusted according to the gradient magnitude. Equation (3) describes this process.

$$\psi(x,y) = \begin{cases} \varrho_{\omega}^{b1} \; if \; \vartheta_c(x,y) \le Th_1; \\ \varrho_{\omega}^{b2} \; Th_1 < \vartheta_c(x,y) \le Th_2; \\ \varrho_{\omega}^{b3} \; Th_1 < \vartheta_c(x,y) \le Th_3; \\ \varrho_{\omega}^{b4} \; otherwise \end{cases} \tag{3}$$

where $\mathbf{\varrho}_{\omega}^{bi}$ $(i = 1, ..., 4)$ are statistical weight coefficients and Th_i is gradient intervals threshold.

3. Now for each block, cumulative weighted gray values are computed as given in Eq. (4).

$$N_g(z) = \sum_{i=1}^{4} \mathbf{\varrho}_{\omega}^{bi} n_i(z) \tag{4}$$

where $n_i(z)$ denotes cumulative value of gray level pixels for each block i.

Three parameters such as maximum region extraction, block size and weighting criteria should be primarily considered for an optimized solution. However, the informative regions are within 25–75%, therefore, considering the minimum value of 25%, the number of blocks selected to be 12 with an aspect ratio of 8:3. For this purpose, the weights assignment is based on number of edge points, E_{pi} for each block as shown in Eq. (5).

$$\omega_{\omega i} = \frac{E_{pi}}{E_{max}^{b}} \tag{5}$$

where E_{max}^{b} is the block with maximum edges.

Before feature vector construction, morphological operations are applied which are series of inter linked steps to make foreground and background maximal differentiable (Duan et al. 2016). The applied morphological operations are closing, filling and reconstruction which efficiently work on all segmented images. These operations are applied on all images to make object/s more distinct with respect to the background.

3.2.3 Feature vector construction

Initially it is agreed that salient regions are unique and maximally differentiable from their background with respect to their textual details and are, therefore, subjected to different texture analysis methods. Here an extended texture features analysis (ETFA) algorithm is utilized. For this purpose, pair threshold binary decomposition (PTBD) will be combined with fuzzy C-means (FCM) algorithm prior to normalization step which is the extension of previous work in which proximal plane clustering is utilized only to produce much better results. A built-in FCM function is applied with a Gaussian membership function. For this purpose, initially the image is divided into stack of binary images and later fractal texture analysis of set of binary images is used based on mean gray levels, boundaries fractal analysis and pixels' count.

3.2.4 Fuzzy C-means and pair threshold binary decomposition

FCM classifies the input data into multiple coherent classes because it is an unsupervised algorithm. This algorithm was introduced by Dunn (1973) and later improved by Bezdek et al. (1984). FCM generates n number of clusters' centers iteratively by adjusting their positions and by evaluating an objective function. This clearly shows that this algorithm

provides high adaptability by allowing one point belonging to multiple clusters with some membership value. Here given a collection of data $X = \{x_i\}_{i=1}^{n}$ where n represents number of samples, $n \in R$ having n samples and are partitioned into c clusters $1 \leq c << n$, the cost function is minimized in Eq. (6):

$$J_m = \sum_{i=1}^{n}\sum_{k=1}^{c} U_{ki}^{m} d^2(x_i, v_k) \tag{6}$$

With constraint of $\sum_{k=1}^{c} U_{ki} = 1$ & $0 \leq U_{ki} \leq 1$, where $U_{ki}$is degree of membership of n^{th} sample point to the c^{th} cluster as in Eq. (7). $m \mid (m \geq 1)$ is a coefficient which controls the fuzziness of algorithm, $d^2(x_i, v_k = \| x_i - v_k \|^2)$ is a distance between cluster center v_k and the sample x_i defined in Eq. (8). $\|$ shows the distance norm. Algorithm 1 presents the FCM algorithm.

$$v_i = \frac{\sum_{i=1}^{n} U_{ki}^{m} x_i}{\sum_{i=1}^{n} U_{ki}^{m}} \tag{7}$$

$$U_{ki} = \frac{1}{\sum_{l=1}^{c} \left(\frac{d_{ki}}{d_{li}}\right)^{\frac{2}{m-1}}} \tag{8}$$

where d_{ki} represents means of the distance $d(x_i, v_k)$.

After that, threshold pair is selected from each cluster label by following upper and lower bounds, referred as thresholds, Th_l^i and Th_u^i. The set of binary images are obtained having upper and lower threshold values, $T = (Th_l^i, Th_u^i)$ as given in Eq. (9).

$$H_b(i,j) = \begin{cases} 1 & if\ Th_l^i \leq H_s(i,j) \leq Th_u^i \\ 0 & otherwise \end{cases} \tag{9}$$

Finally, $H_b(i,j)$ is utilized for construction of feature vector.

Algorithm1 FCM Algorithm

1: Required: Input data X with number of clusters c, parameter m and stop criteria $\in$, where I is the iteration step
2: Initialize $U = [u_{ik}]\ matrix, U^{[0]}$
3: At step I, calculate U_i and V_i using Equations 5 and 6
4: Update $V_i, V_{(i+1)}$ using Equation 5
5: Repeat steps 2 and 3 until $\| U^{(l+1)} - U^{(l)} \| < \varepsilon$

3.2.5 Extended features texture analysis (EFTA)

Once the dermoscopic binary images $Th = (Th_l^i, Th_u^i)$ are obtained, the features are extracted based on pixels' count, boundaries fractal dimension and mean gray level. Algorithm 2 describes the process of EFTA. A set of threshold values are produced by including FCM algorithm with multiple thresholds. The regions boundaries for each binary image which is represented by $\psi(i,j)$, are computed as follows in Eq. (10):

$$\psi_{i,j} = \begin{cases} 1, & if\ (x', y') \in N_8[(x,y)] \\ & H_b(x,y) = 0 \wedge H_b(x,y) = 1 \\ 0, & otherwise \end{cases} \tag{10}$$

where $N_8[(x,y)]$ represents 8-connected pixels, $\psi_{i,j}$ produces 'True' value if a pixel at position (x,y) in $H_b(x,y)$ produces 'True' with minimum single 'False' at its neighbors otherwise it will be 0. Like perimeter method, fractal dimensions can be computed with the utilization of box counting algorithm. The Hausdorffs fractal dimension E_o is computed using following expression in Eq. (11).

$$E_o = \lim_{\in \to 0} \frac{\log N(\varepsilon)}{\log \varepsilon^{-1}} \tag{11}$$

Algorithm 2 ETFA Algorithm

1: **Required:** Input RGB/Gray Image $\mathcal{V}_c(x,y)$ and number of thresholds Th_i
2: At step I, calculate U_i and V_i using Equations 5 and 6
3: Update $V_i, V_{(i+1)}$ using Equation 5
4: Repeat steps 2 and 3 until $\| U^{(l+1)} - U^{(l)} \| < \varepsilon$

To select the final image, initially nine color channels are processed and four channels are ignored based on maximum and minimum details. The core reason is that the channels with minimum details discard the relevant information whilst channels with maximum details provide irrelevant information. After omitting four color channels, the rest of five channels participate in the final selection process based on weights calculated using distance from the center (w_{dc}), number of connected components (w_{cl}), boundary connection (w_{bc}) and distance matrix (w_{dm}). Therefore, the cumulative weight relies on four conditions mentioned below in Eq. (12):

$$w_{final} = w_{dc} + w_{bc} + w_{cl} + w_{dm} \tag{12}$$

3.2.6 Evaluation of segmentation results

In this section, segmentation results are presented both in tabular and visual formswhich reveal the authenticity of proposed method. Three benchmark data sets, PH2 (Bi et al. 2016), ISIC and ISBI 2016 (Gutman et al. 2016) are utilized to measure the segmentation accuracy in which ground truth images are already verified by an expert dermatologist. Proposed algorithm is tested on random image samples from each data set, results can be seen in Figs. 4 and 5. For the demonstration purpose, only few image samples from three data sets are provided in the form of table along with their accuracies.

In the first phase, the proposed segmentation method is tested on PH2 data set that consists of 200 images.

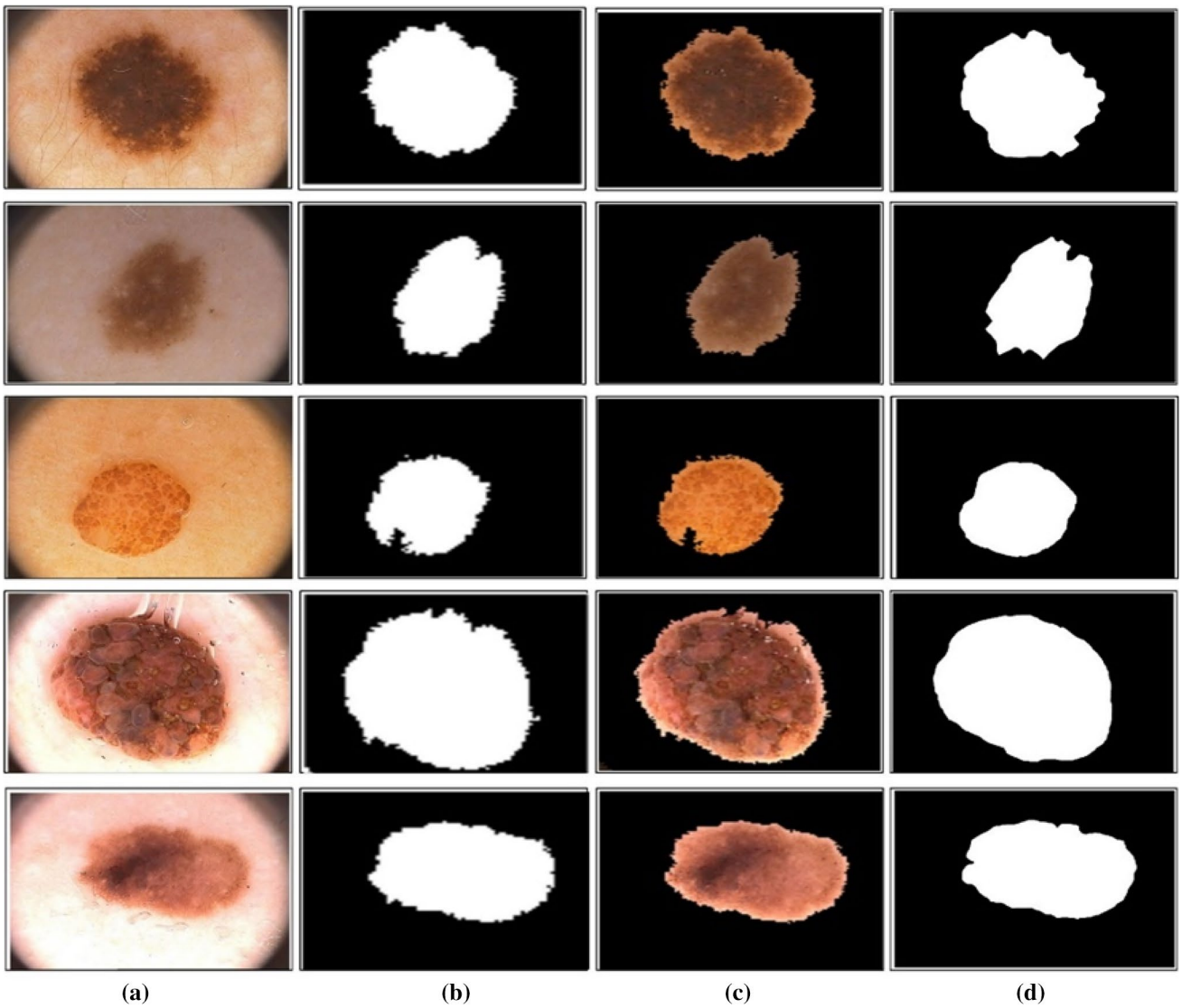

Fig. 4 Proposed lesion segmentation effects on PH2 data set: **a** RGB image; **b** proposed lesion extraction; **c** mapped proposed segmented image on original RGB image; **d** corresponding ground truth

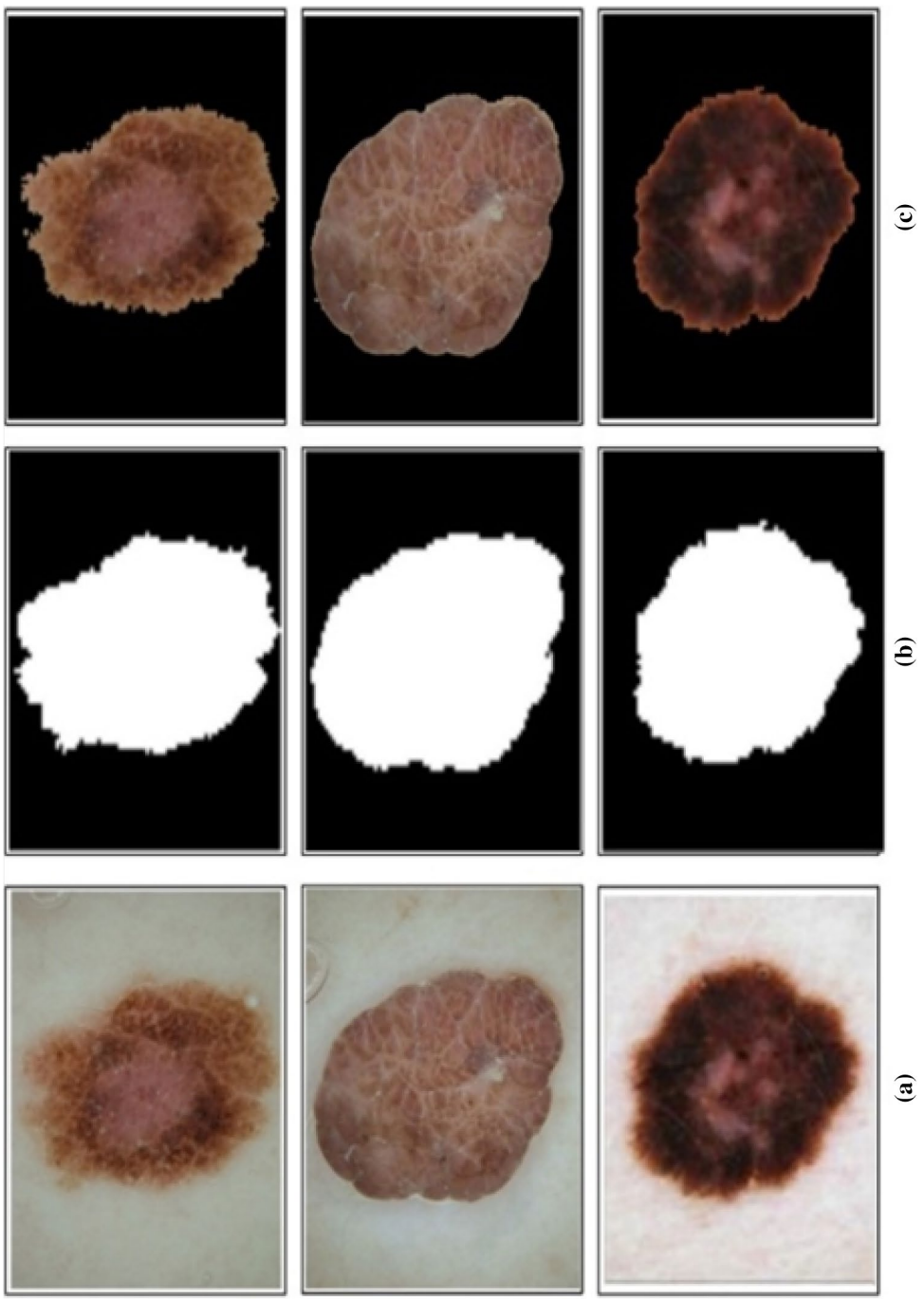

Fig. 5 Proposed segmentation effects on ISIBI 2016 data set: **a** original image; **b** proposed lesion segmentation; **c** mapped on original image

Table 1 Proposed segmentation accuracy on PH2 and ISBI 2016 data sets

PH2 data set		ISBI 2016 data set		ISIC data set	
Image no.	Accuracy (%)	Image no.	Accuracy (%)	Image no.	Accuracy (%)
IMD002	93.67	1	90.12	1	90.21
IMD007	93.27	2	90.45	2	90.56
IMD018	92.65	3	90.49	3	91.99
IMD029	90.99	4	89.99	4	91.89
IMD036	92.22	5	92.23	5	91.31
IMD049	93.33	6	92.67	6	93.67
IMD060	92.22	7	92.99	7	95.30
IMD069	89.54	8	88.87	8	97.21
IMD082	90.77	9	88.35	9	89.99
IMD094	93.39	10	90.66	10	94.37
IMD103	92.14	11	93.35	11	95.54
IMD109	93.12	12	94.44	12	95.55
IMD117	88.13	13	95.51	13	95.99
IMD149	89.92	14	95.01	14	94.10
IMD168	94.32	15	96.65	15	92.22
IMD173	94.13	16	90.34	16	92.89
IMD189	94.45	17	86.58	17	92.90
IMD199	89.24	18	89.93	18	90.19
IMD207	92.11	19	88.94	19	90.99
IMD220	94.26	20	90.34	20	91.94
IMD238	94.44	21	94.35	21	96.76
IMD349	95.32	22	93.26	22	95.55
IMD370	92.99	23	94.35	23	94.38
IMD380	92.45	24	88.45	24	96.39
IMD399	94.65	25	89.93	25	90.17
Average	92.54	Average	91.53	Average	93.2824

The proposed method performs well on PH2 data set and achieves an average accuracy of more than 90%. Top 25 results are presented in Table 1. Similarly, in the second phase, ISBI 2016 data set is utilized that consists of more than 900 images. The achieved average accuracy on all images of ISBI 2016 data set is above 91% and top 25 images results are shown in Table 1. In the third phase, ISIC data sets such as MSK and UDA are utilized having total 3,252 images and achieved overall average accuracy above 90%. Few numerical results are given in Table 1.

It is clear from the statistics that with proposed segmentation results, maximum accuracy for the set of selected images (ISBI 2016) is 95.32% while average accuracy achieved is 92.54% which is comparable to Bi et al. (2016) in which reported maximum segmentation accuracy is 92.49%.

3.3 Feature extraction

Feature extraction is one of the most important steps in the field of machine learning on which classification accuracy truly relies upon. In this step, image is transformed into low dimensional sub space that contains more relevant information about an object (Amin et al. 2017a; Khalid et al. 2014). Features play their vital role in multiple domains for precise classification including action classification (Khan et al. 2018b; Sharif et al. 2017), person re-identification (Shah et al. 2017a), skin lesion classification(Nasir et al. 2018), MRI images (Amin et al. 2017b), stomach infections (Liaqat et al. 2018), agricultural diseases (Iqbal et al. 2018) and many more (Khan et al. 2017; Raza et al. 2018; Sharif et al. 2018a, b). Moreover, few additional steps of feature reduction and selection are also gaining much importance in machine learning community to acquire improved classification accuracy because of the selection of only relevant information and removing the redundant features.

In this section, features are extracted for the classification of melanoma and benign from selected images. The features are calculated from color and segmented lesion images. The segmentation step gives guarantee about lesion and the background; therefore, the objective here is to extract a set of robust features that accurately describe each lesion and ensure the melanoma and benign. For this purpose, ABCDE and shape features are extracted in the proposed technique for lesion classification. The ABCDE features are

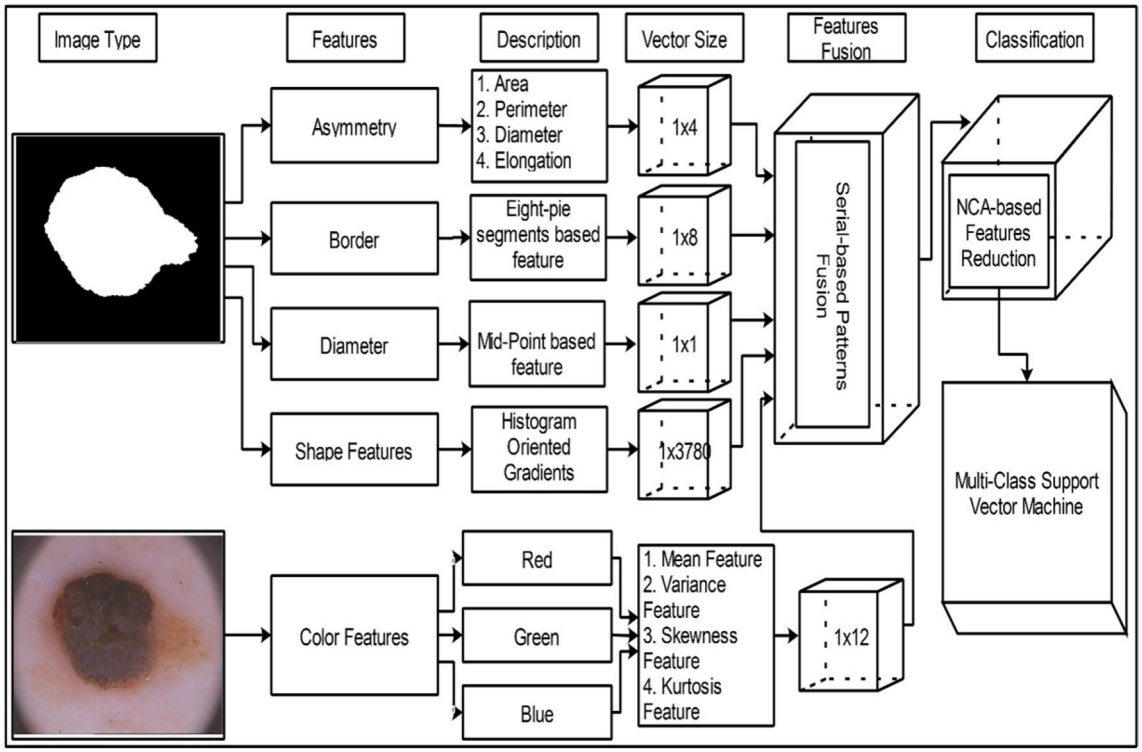

Fig. 6 Flow diagram of proposed feature extraction, reduction and classification steps

well known and famous dermoscopic descriptors known as asymmetry (A), border irregularity (B), color (C), diameter (D) and evaluation (E) but E is not utilized because the evolution helps a dermatologist and a patient to observe the severity stage of melanoma and take prognostic measures at the earliest. This process is performed by classifier at final stage in terms of classification. Thereafter, the extracted features are fused by a serial based method to combine the pattern information of all features in a single vector. The dimensionality of fused vector is reduced by neighborhood feature component analysis (NFCA) method and classified by multi-class SVM (M-SVM). The detailed description of each step is in Fig. 6 below.

3.3.1 Asymmetry

Asymmetry of lesion is determined with the help of shape features which are calculated based on lesion area, lesion perimeter, lesion equivalent diameter and elongation. Asymmetry of a lesion is determined by dividing the lesion into horizontal and vertical axes. Asymmetry index is calculated by defining the principal axes of symmetry of lesion $I(\varphi)$, crossing the centre of gravity with a angle φ to the horizontal axis (Ahnlide et al. 2016). Equation (13) defines this:

$$I(\varphi) = \sum_{(i,j)\in L} D_{\varphi}^{2} = \sum_{(i,j\in L)} \left[-i\sin(\varphi) + j\cos\varphi\right] \tag{13}$$

where D_{φ} is the distance between current pixel (i, j) and horizontal projection, φ is obtained by computing the derivative of Eq. (11) and setting it to zero as expressed in Eq. (14).

$$\frac{\partial I(\varphi)}{\partial \varphi} = 0 \Rightarrow \varphi_0 = \frac{1}{2}\arctan\left[\frac{2m_{11}^{s}}{m_{20}^{s} - m_{02}^{s}}\right] \tag{14}$$

The m_{11}^{s}, m_{20}^{s} and m_{02}^{s} represent the standard product moments. Area of lesion is measured by following Eq. (15).

$$A = \frac{1}{2}\sum_{k=1}^{2}\frac{\Delta A_k}{A_q} \tag{15}$$

where subscript k represents the principal axes (major vs. minor) depending on the rotation, ΔA_k is the corresponding non-overlapping area of lesion and A_q ($A_q = m_{00}^{s}$) is the lesion area. The perimeter of lesion is determined by the inter connections of similar pixels at the boundaries of lesion. The connectivity relation is determined by finding the connectivity between two pixels by 4-connected (N_4) and 8-connected (N_8) methods.

3.3.2 Border

The lesion is divided into eight segments to examine if there is any abrupt and distinctive cut off. The border irregularity

is defined to be edge protrusion, scratched and blurred. The border irregularities can be computed by Eq. (16).

$$B = \frac{P^2}{4\pi A} \tag{16}$$

where P is the perimeter of lesion boundary calculated as $P = 2L + 2W$. L and W are length and width of segmented lesion and A is the lesion area.

3.3.3 Diameter

The melanomas grow after inception and tend to protrude than common body nevi which is considered very risky if greater than 5 mm. The method is adopted to find the diameter threshold by determining cross diameters through the midpoint from entire edge pixels and then calculating their mean. Diameter of lesion is determined as in Eq. (17).

$$D = 2a \tag{17}$$

where a is a semi major axis of best fit ellipse.

3.3.4 Color features

In medical imaging, color features are most importantly used by dermatologist for the classification of skin lesions (Barata et al. 2014). The color features distinguish granularity between melanoma and benign (Stoecker et al. 2011). They contain complete information of an RGB image which contributes in differentiating the lesion classes (Permuter et al. 2006). The lesion color varies with different shades of brown, black, red, white and blue. Therefore, for this purpose, RGB color space is used in the proposed method and its three components like red, green and blue are extracted. These channels are expressed as follows from Eqs. (18) to (20).

$$\gamma_r = \frac{\sigma_r}{Max_r} \tag{18}$$

$$\gamma_g = \frac{\sigma_g}{Max_g} \tag{19}$$

$$\gamma_b = \frac{\sigma_b}{Max_b} \tag{20}$$

where σ represents standard deviation in every color channel and max denotes the maximum value of different color channels in lesion. Thereafter, four different statistical parameters such as mean, variance, skewness and kurtosis are extracted. These parameters generate a single value for each channel and later on combine their information in a vector. The size of output color feature vector is 1×12 which contains pattern information for all channels. These parameters are expressed as follows from Eqs. (21) to (24).

$$\mu = \frac{1}{N}\sum_{i=1}^{N} x_i \tag{21}$$

$$\sigma^2 = \frac{\sum x^2}{N} - \mu^2 \tag{22}$$

$$Sk = \frac{\sum_{i=1}^{N} (x_i - \bar{x})^3 / N}{\sigma^3} \tag{23}$$

$$Kr = \frac{\sum_{i=1}^{N} (x_i - \bar{x})^4 / N}{\sigma^4} - 3 \tag{24}$$

where μ denotes mean feature, σ^2 is variance feature, Sk is skewness feature, Kr is kurtosis feature, N represents total number of pixels in each extracted channel like γ_r, γ_g and γ_b.

3.3.5 Histogram of oriented gradient features (HOG)

Histogram of oriented gradient features also known as shape based features are originally designed for human detection in the domain of pattern recognition (Dalal and Triggs 2005). They contain local shape information which covers the distribution of local intensity and edges directions of objects in query images. The computation of HOG features is completed in four steps. In the first step, gradient is computed which represents the directional information of an image. In the second step, cell histogram is considered according to which blocks are created in the third step. Finally, the blocks are normalized based on L2-normalization. The size of an extracted vector is 1×3780 which is later fused by a serial based method.

3.3.6 Features fusion and reduction

Different feature extraction and reduction techniques (Shah et al. 2017b) exhibit different visual characteristics; therefore, the utilization of multiple features allows exploiting the strengths for improved classification accuracy. Hence primary objective here is to improve the classification performance while combining multiple features such as shape, color and texture. These features save distinct information about objects; therefore the fusion of these features in one vector gives better object information. In the presented technique, a low level fusion approach is adopted by directly concatenating the extracted features to construct a joint feature space. A serial based method is implemented to fuse all features in one vector. The serial method is defined as follows in Eq. (25):

$$FV = FV1_i + FV2_j + FV3_k + FV4_l + FV5_m \tag{25}$$

where FV denotes the fused feature vector, $FV1$, $FV2$, $FV3$, $FV4$ and $FV5$ are extracted features such as asymmetry, border, diameter, shape and color. The sizes are $i = 4$, $j = 8$, $k = 1$, $l = 3780$ and $m = 12$ respectively. Hence the size of fused vector is 1×3805. Afterwards, dimensions are reduced using NCA method (Goldberger et al. 2005). NCA is one of supervised distance learning metric algorithms which can learn from both samples and their labels (Goldberger et al. 2005). The main objective of this algorithm is to acquire a conversion matrix that exploits the performance of KNN classification (Qin et al. 2015). For this purpose, NCA needs to optimize the expected leave-one-out (LOO) error of a stochastic KNN classifier in the projection space induced by this transformation. NCA for feature selectionfinds weighting vector that confers itself to select the feature sub set optimizing classification task (Yang et al. 2012). The reduced features obtained after NCA reduction are later classified by M-SVM (Liu and Zheng 2005).

4 Experimental results and discussion

4.1 Implementation

In this proposed methodology, multiple modules (self-programmed and open source) are integrated as per requirement. In the preprocessing section, from channels separation to weights calculation, code is almost developed by the authors except EFTA algorithm which is open source software and Fuzzy C-means—built-in MATLAB function. Similarly, in the feature extraction phase, border and shape features (HOG) are calculated from built-in MATLAB commands. The proposed model is implemented in MATLAB, R2017b using a desktop computer having 16 GB of RAM, GPU of Sapphire R9-290 X Tri-X OC Edition with 4 Gigabytes of DDR5 373 Video RAM. For lesion classification, built-in image category classifier is implemented which takes advantage of installed GPU for final categorization. Simulation results on each data set are provided in detail in the forthcoming sections.

4.2 Evaluation protocols

Three benchmark data sets including ISBI 2016, PH2 and ISIC are used for the evaluation of proposed system. These data sets contain RGB images, where the images dimension of each data set is different from each other. The evaluation results are computed on M-SVM and their performance is compared with seven other classification methods such as linear discriminant analysis (LDA), linear regression (LR), complex tree (CT), W-KNN, Naive Bayes, ensemble boosted tree (EBT) and ensemble subspace discriminant analysis (ESDA). Performance of each classifier is calculated using eight statistical measures including sensitivity (sen), specificity (spec), precision (prec), false positive rate (FPR), negative predicted value (NPV), false negative rate (FNR), accuracy and execution time.

4.3 ISBI 2016 data set

ISBI 2016 skin lesion data set consists of total 1279 RGB images having 273 melanomas and 1006 benign. For the evaluation of proposed method, an approach of 50:50 for training and testing is opted. The 10-fold crossvalidation is used for the evaluation of each selected classifier. The best accuracy is 99.2%, sensitivity 99.2%, specificity

Table 3 Confusion matrix for ISBI 2016 data set

Confusion matrix for ISBI 2016 data set				
Classification class	Total testing images	Classification class		
		Benign (%)	Melanoma (%)	TPR (%)
Benign	503	**99.4**	0.6	99.4
Melanoma	136	1	**99**	99

Bold values shows the significant results

Table 2 Classification results of ISBI 2016 data set

Method	Measures							
	FPR	Sen (%)	Spec (%)	Prec (%)	NPV (%)	FNR (%)	Accuracy (%)	Ex time/s
CT	0.020	98.0	98.0	98.0	2.0	1.9	98.1	14.115
LDA	0.015	98.5	99.0	98.5	1.5	1.4	98.6	5.724
LR	0.360	64.0	58.0	64.5	35.5	35.8	64.2	27.09
W-KNN	0.015	98.5	99.0	98.5	1.5	1.3	98.7	3.158
NB	0.015	98.5	99.0	98.5	1.5	1.4	98.6	4.082
EBT	0.015	98.5	99.0	98.5	1.5	1.0	99.0	10.591
ESDA	0.015	98.5	99.0	98.5	1.5	1.4	98.6	14.115
M-SVM	**0.005**	**99.2**	**99.4**	**99.4**	**0.6**	**0.8**	**99.2**	**2.972**

Bold values shows the significant results

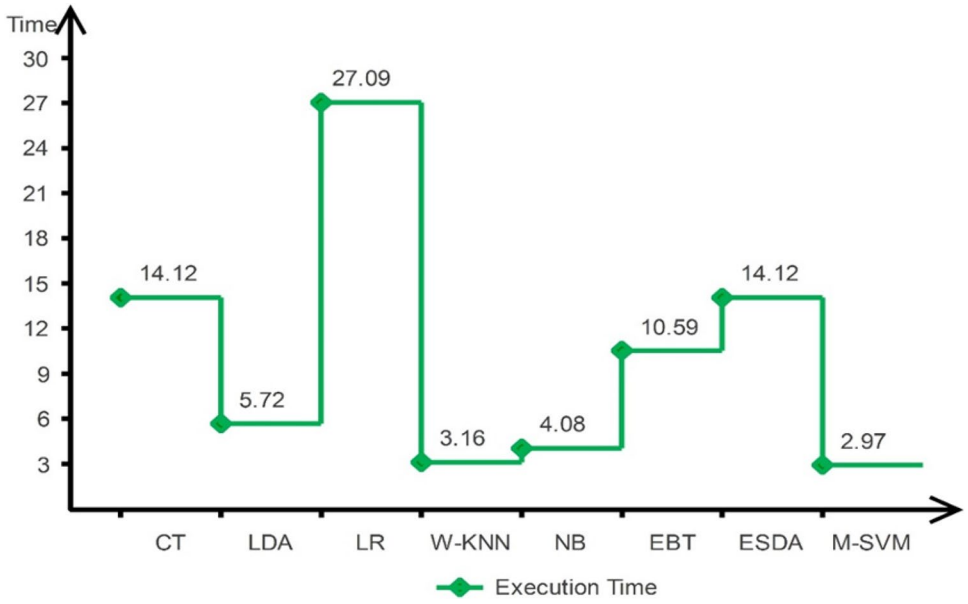

Fig. 7 Execution time of proposed method for selected classification methods on ISBI 2016 data set

Table 4 Classification results of PH2 data set

Method	Measures							
	FPR	Sen (%)	Spec (%)	Prec (%)	NPV (%)	FNR (%)	Accuracy (%)	Ex time/s
CT	0.097	77.33	86.0	77.6	22.33	19.0	81.0	2.166
LDA	0.021	95.00	97.5	95.0	5.00	4.0	96.0	1.624
LR	0.023	95.33	96.5	94.0	6.00	4.5	95.5	1.320
W-KNN	0.033	92.33	97.0	93.0	7.00	6.0	94.0	1.112
NB	0.026	93.67	96.5	93.0	7.00	5.5	94.5	1.724
EBT	0.033	92.00	96.5	92.6	7.33	6.5	93.5	2.23
ESDA	0.016	**96.67**	97.5	95.6	4.33	3.0	97.0	2.427
M-SVM	**0.010**	96.30	**99.5**	**97.3**	**2.70**	**2.5**	**97.5**	**0.901**

Bold values shows the significant results

Table 5 Confusion matrix for PH2 data set

Confusion matrix for PH2 data set					
Classification class	Total testing images	Classification class			
		Benign	Common nevi (%)	Melanoma (%)	TPR (%)
Benign	40	**99.0**	–	1.0	99.0
Common nevi	40	–	**100**	–	100
Melanoma	20	10%	–	**90**	90

Bold values shows the significant results

99.4%, precision 99.4%, NPV 0.6, FNR 0.8% and FPR is 0.005 achieved on M-SVM as given in Table 2. The M-SVM accuracy is proved by Table 3 which presents its confusion matrix. Moreover, the execution time is calculated on all classification methods and shows that M-SVM outperforms other approaches in Table 2. The execution time comparison with existing classification methods is also shown in Fig. 7. From Fig. 7, it is clear that the proposed method performed efficiently on M-SVM with execution time 2.973 s.

4.4 PH2 dataset

This data set comprises of total 200 RGB images having 80 benign, 80 basal cell carcinoma and 40 melanomas. For

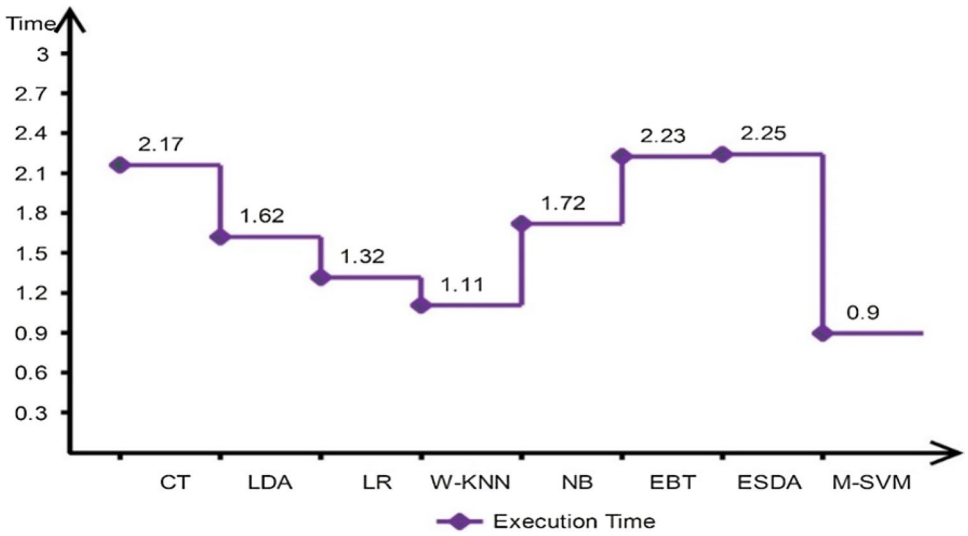

Fig. 8 Execution time of proposed method for selected classification methods on PH2 data set

Table 6 Classification results of ISIC-UDA data set

Method	Measures							
	FPR	Sen (%)	Spec (%)	Prec (%)	NPV (%)	FNR (%)	Accuracy (%)	Ex time/s
CT	0.22	78.0	96.0	85.0	15.0	11.1	88.9	9.847
LDA	0.04	96.0	97.0	93.5	6.5	3.5	96.5	6.304
LR	0.19	81.0	82.0	73.5	26.5	18.2	81.8	15.199
W-KNN	0.04	96.0	97.0	94.5	5.5	3.0	97.0	2.721
NB	0.05	94.5	94.0	89.0	11.1	6.1	93.9	2.445
EBT	0.08	92.5	97.0	93.5	6.5	4.5	95.5	6.469
ESDA	0.05	95.0	97.0	94.0	6.0	3.5	96.5	5.778
M-SVM	**0.01**	**99.0**	**100**	**99.5**	**0.5**	**0.5**	**99.5**	**2.103**

Bold values shows the significant results

Table 7 Confusion matrix for ISIC-UDA data set

Confusion matrix for ISIC-UDA data set				
Classification class	Total testing images	Classification class		
		Benign (%)	Melanoma (%)	TPR (%)
Benign	308	**100**	–	100
Melanoma	58	3.0	**98**	98

Bold values shows the significant results

the evaluation, images are resized into 256 × 256 and an approach of 50:50 is used for system training and testing. 10-fold crossvalidation is performed for testing results. The proposed method achieved best testing accuracy 97.5%, specificity 99.5%, precision rate 97.3%, NPV 2.7%, FNR 2.5% and FPR is 0.010 on M-SVM as given in Table 4 and proved by Table 5. From Table 4, the best sensitivity rate is 96.67% which is achieved on ESDA classifier. Moreover, as execution time is more important for real time applications, therefore, the testing execution time for each classifier is calculated and given in Table 4. The execution of M-SVM is best (0.901 s) as compared to other classification methods as shown in Fig. 8. From the above discussion and Table 4, it is clear that M-SVM outperforms. Also, ESDA and LDA achieved second and third best accuracy on PH2 data set.

4.5 ISIC data base

The ISIC is an academia and industry partnership which helps to reduce the melanoma morality rate. The ISIC consists of several benchmark data sets such as MSK-1, MSK-2, ISIC-UDA and HAM10000. From these, ISIC UDA and ISIC MSK1 & MSK2 are selected for evaluation. The detailed results are given below.

4.5.1 ISIC UDA

ISIC UDA data base consists of total 617 RGB dermoscopic images having dimensions 1022 × 1022, 1504 × 1504,

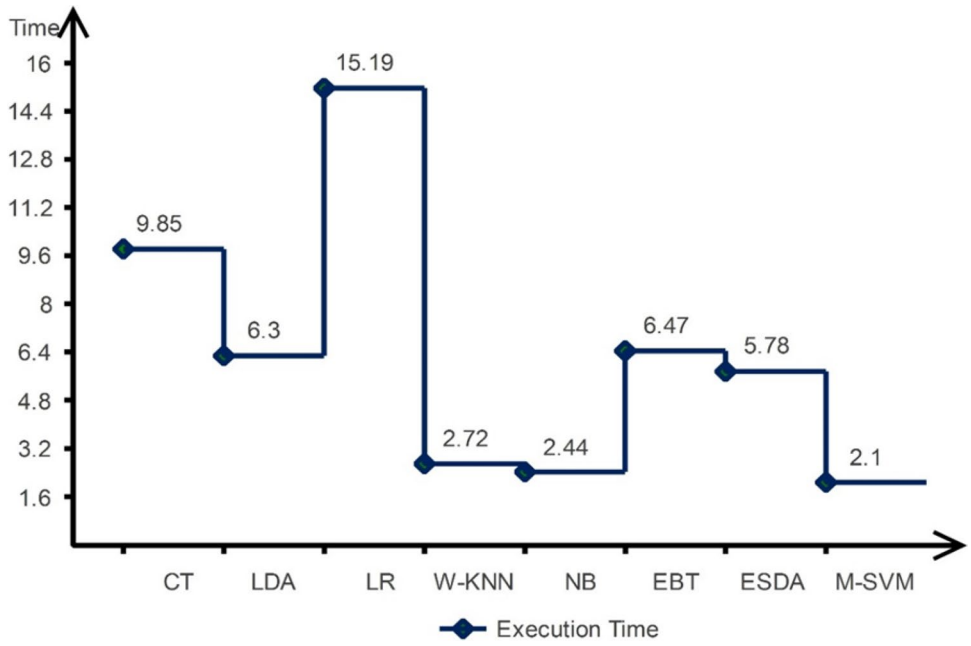

Fig. 9 Execution time of proposed method for selected classification methods on ISIC UDA data set

Table 8 Classification results of ISIC-MSK 1&2 data set

Method	Measures							
	FPR	Sen (%)	Spec (%)	Prec (%)	NPV (%)	FNR (%)	Accuracy (%)	Ex time/s
CT	0.120	88.0	96.0	89.0	10.5	7.1	92.9	13.180
LDA	0.035	97.0	96.0	93.0	7.0	3.5	96.5	5.305
LR	0.125	87.5	85.0	79.0	21.0	13.6	86.4	15.305
W-KNN	0.050	95.0	97.0	93.0	7.0	4.0	96.0	4.009
NB	0.155	85.0	92.0	82.0	18.0	11.1	88.9	2.318
EBT	0.070	93.5	**99.0**	97.0	3.0	3.0	97.0	6.664
ESDA	0.030	97.5	97.0	95.0	5.0	2.5	97.5	7.663
M-SVM	**0.02**	**98.5**	**99.0**	**98.5**	**1.5**	**1.0**	**99.0**	**2.012**

Bold values shows the significant results

Table 9 Confusion matrix for ISIC-MSK 1&2 data set

Confusion matrix for ISIC-MSK 1&2 data set				
Classification class	Total testing images	Classification class		
		Benign (%)	Melanoma (%)	TPR (%)
Benign	800	**99.0**	1.0	99
Melanoma	517	3.0	**98**	98

Bold values shows the significant results

962 × 962 and few more. The total images consist of 187 melanomas and 430 benign. A 50:50 approach is selected for system training and testing which explains that 93 melanoma and 215 benign images are used for training the classifier and remaining images are utilized for testing. The best testing classification accuracy achieved is 99.5%, sensitivity 99.0%, specificity 100%, FNR 0.5% and FPR is 0.01 on M-SVM as presented in Table 6. Table 7 presents confusion matrix which proves the classification accuracy of M-SVM for the proposed method. The second highest classification accuracy is 97.0% achieved on W-KNN. The system execution time is also provided in Table 6 for all selected classifiers. Moreover, the best execution time is 2.103 s which is achieved on M-SVM as shown in Fig. 9. Keeping in view all above and results, it is clear that M-SVM performed best as compared to other listed classification methods.

4.5.2 ISIC MSK 1&2 data base

ISIC MSK data base consists of total 2635 RGB dermoscopic images having dimensions 1024 × 1024. This data base includes five different sub data sets such as MSK-1, MSK-2, MSK-3, MSK-4 and MSK-5. In the proposed method, MSK-1 and MSK-2 data bases are selected for

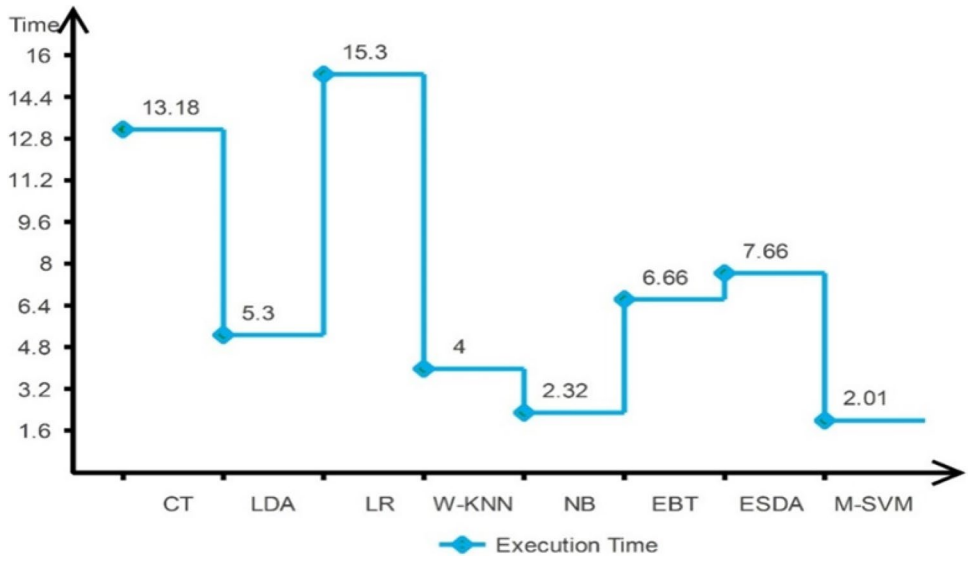

Fig. 10 Execution time of proposed method for selected classification methods on ISIC MSK 1&2 data set

the evaluation of proposed method. The combination of MSK-1 and MSK-2 data bases consists of total 2635 dermoscopic images, where all images are in RGB format. To calculate the classification results, a ratio of 50:50 is chosen for training and testing. The maximum testing classification accuracy is 99.0% which is achieved on M-SVM. Similarly, sensitivity is 98.5%, specificity 99.0%, precision rate 98.5% and FPR is 0.020 achieved on M-SVM as given in Table 8 which is proved by Table 9. Moreover, the testing execution time of proposed method is given in Table 8 showing that M-SVM performed fast as compared to other classification methods as shown in Fig. 10. In view of above arguments, proposed method performed well for ISIC MSK 1&2 data set on M-SVM in terms of calculated statistical parameters.

4.6 Discussion

In this section, proposed lesion segmentation and classification method is discussed in terms of visual and numerical analysis. With the fact that manual segmentation and classification of skin lesion is quite difficult and time consuming job, researchers introduced computer based systems that automatically segment and classify skin lesions and assign a label to them as depicted in Fig. 1. In the proposed method, firstly saliency method is implemented for lesion segmentation as shown in Figs. 4 and 5. The evaluation of saliency method is performed on three publicly available data sets ISBI 2016, PH2 and ISIC by achieving an average accuracy of more than 90%. Few selected segmentation results are presented in Table 1, where average segmentation accuracy on PH2 data set is 92.54%, ISBI 2016 is 91.53%, ISIC UDA is 99.5% and ISIC MSK1 & MSK 2 is 99%. Thereafter, clinical, shape and color features are extracted

Table 10 Comparison with existing methods for ISBI 2016 and PH2 data sets

Method	Data sets	Year	Comparison measures				
			Sensitivity (%)	Specificity (%)	Precision (%)	Accuracy (%)	Ex time/s
Adjed et al. (2017)	PH2	2017	78.93	93.25	–	86.07	–
Waheed et al. (2017)	PH2	2017	97.0	84.0	–	96.0	–
Bozorgtabar et al. (2016)	ISBI 2016	2016	–	–	86.0	–	–
Lopez et al. (2017)	ISBI 2016	2017	78.66	–	79.74	81.33	–
Yu et al. (2017)	ISBI 2016	2017	54.70	93.10	62.40	85.50	–
Majtner et al. (2016)	ISBI 2016	2016	53.30	89.80	–	82.60	–
Proposed	ISBI 2016	2018	99.40	99.20	99.40	99.20	2.972
	PH2	2018	96.30	99.50	97.30	97.50	0.901
	UDA	2018	99.0	100	99.50	99.50	2.103
	MSK1 & MSK 2	2018	98.50	99.0	98.50	99.0	2.012

from segmented and RGB images. The extracted features are fused by employing serial based technique that is later reduced using NCA reduction approach. Finally, the reduced features are classified using M-SVM by achieving average accuracy of 99.2%, 97.5%, 99.5% and 99.0% using M-SVM, presented in Tables 2, 4, 6 and 8. Classification results can also be confirmed from confusion matrices in Tables 3, 5, 7 and 9. An important parameter of execution time is also being added for each data set, shown in Fig. 7, 8, 9 and 10. These graphical representations clearly show that M-SVM performed much better as compared to other supervised learning methods such as W-KNN, EBT and LDA to name a few. Moreover, a general comparison with other recent techniques is also conducted, Table 10, to authenticate the accuracy of proposed method.

It is clear from Table 10 that achieved classification accuracy of 86.07%, sensitivity 78.93% and specificity 93.25% (Adjed et al. 2017) improved classification accuracy up to 96% with sensitivity rate 97% and specificity 84% (Waheed et al. 2017).Whereas, the proposed achieved classification accuracy is 97.5% with sensitivity 96.30%, specificity 99.50% and precision rate 97.30%. Moreover, the classification accuracy on ISBI 2016 is also calculated. The proposed classification accuracy on ISBI 2016 data set is 99.20% which is significantly well as compared to existing methods. Similarly on ISIC data sets (UDA, MSK1 & MSK2), the achieved classification accuracy is 99.5% and 99% respectively.

5 Future work

Recently, deep learning has gained much attention from machine intelligence community. They performed successfully deep learning algorithms in computer vision domain such as skin lesion classification (Kawahara et al. 2016), action recognition (Uddin et al. 2017), contentbased image retrieval (CBIR) (Alzu'bi et al. 2017) etc. Particularly, convolutional neural network (CNN) architectures have demonstrated improved performance to encode available image information. In CNN, high level features are learned in deeper layers and combinations of low level features are determined in the shallow layers. Therefore, in future, CNN based approach can be implemented and tested on ISBI 2017.

References

Adjed F, Gardezi SJS, Ababsa F, Faye I, Dass SC (2017) Fusion of structural and textural features for melanoma recognition. IET Comput Vis 12(2):185–195

Ahnlide I, Bjellerup M, Nilsson F, Nielsen K (2016) Validity of ABCD rule of dermoscopy in clinical practice. Acta dermato Venereol 96(3):367–372

Aksac A, Ozyer T, Alhajj R (2017) Complex networks driven salient region detection based on superpixel segmentation. Pattern Recognit 66:268–279

Al-Ayyoub M, Al-Mnayyis N, Alsmirat MA, Alawneh K, Jararweh Y, Gupta BB (2018) SIFT based ROI extraction for lumbar disk herniation CAD system from MRI axial scans. J Ambient Intell Humaniz Comput, 1–9

Alzu'bi A, Amira A, Ramzan N (2017) Content-based image retrieval with compact deep convolutional features. Neurocomputing 249:95–105

Amin J, Sharif M, Yasmin M, Ali H, Fernandes SL (2017a) A method for the detection and classification of diabetic retinopathy using structural predictors of bright lesions. J Comput Science 19:153–164

Amin J, Sharif M, Yasmin M, Fernandes SL (2017b) A distinctive approach in brain tumor detection and classification using MRI. Pattern Recognit Lett. https://doi.org/10.1016/j.patrec.2017.10.036

Ansari UB, Sarode T (2017) Skin cancer detection using image processing. Int Res J Eng Technol 4(4):2875–2881

Arroyo JLG, Zapirain BG (2014) Detection of pigment network in dermoscopy images using supervised machine learning and structural analysis. Comput Biol Med 44:144–157

Barata C, Ruela M, Francisco M, Mendonça T, Marques JS (2014) Two systems for the detection of melanomas in dermoscopy images using texture and color features. IEEE Syst J 8(3):965–979

Bezdek JC, Ehrlich R, Full W (1984) FCM: The fuzzy c-means clustering algorithm. Comput Geosci 10(2–3):191–203

Bi L, Kim J, Ahn E, Feng D, Fulham M (2016) Automated skin lesion segmentation via image-wise supervised learning and multi-scale superpixel based cellular automata. In: Paper presented at the biomedical imaging (ISBI), 2016 IEEE 13th international symposium on

Bokhari F, Syedia T, Sharif M, Yasmin M, Fernandes SL (2018) Fundus image segmentation and feature extraction for the detection of glaucoma: a new approach. Curr Med Imaging Rev 14(1):77–87

Bozorgtabar B, Abedini M, Garnavi R (2016) Sparse coding based skin lesion segmentation using dynamic rule-based refinement. In: Paper presented at the international workshop on machine learning in medical imaging

Brunssen A, Waldmann A, Eisemann N, Katalinic A (2017) Impact of skin cancer screening and secondary prevention campaigns on skin cancer incidence and mortality: a systematic review. J Am Acad Dermatol 76(1):129–139. e110

Busin L, Vandenbroucke N, Macaire L (2008) Color spaces and image segmentation. Adv Imaging Electron Phys 151(1):1

Capdehourat G, Corez A, Bazzano A, Alonso R, Musé P (2011) Toward a combined tool to assist dermatologists in melanoma detection from dermoscopic images of pigmented skin lesions. Pattern Recogn Lett 32(16):2187–2196

Codella NC, Gutman D, Celebi ME, Helba B, Marchetti MA, Dusza SW, Kittler H (2018) Skin lesion analysis toward melanoma detection: a challenge at the 2017 international symposium on biomedical imaging (ISBI), hosted by the international skin imaging collaboration (ISIC). In: Paper presented at the biomedical imaging (ISBI 2018), 2018 IEEE 15th international symposium on

Dalal N, Triggs B (2005) Histograms of oriented gradients for human detection. In: Paper presented at the computer vision and pattern recognition, 2005. CVPR 2005. IEEE computer society conference on

Dalila F, Zohra A, Reda K, Hocine C (2017) Segmentation and classification of melanoma and benign skin lesions. Opt Int J Light Electron Opt 140:749–761

Dhane DM, Krishna V, Achar A, Bar C, Sanyal K, Chakraborty C (2016) Spectral clustering for unsupervised segmentation of lower extremity wound beds using optical images. J Med Syst 40(9):207

Dhane DM, Maity M, Mungle T, Bar C, Achar A, Kolekar M, Chakraborty C (2017) Fuzzy spectral clustering for automated delineation of chronic wound region using digital images. Comput Biol Med 89:551–560

Duan Q, Akram T, Duan P, Wang X (2016) Visual saliency detection using information contents weighting. Opt Int J Light Electron Opt 127(19):7418–7430

Dunn JC (1973) A fuzzy relative of the ISODATA process and its use in detecting compact well-separated clusters. J Cybern 3:32–57. https://doi.org/10.1080/01969727308546046

Eltoukhy MM, Elhoseny M, Hosny KM, Singh AK (2018) Computer aided detection of mammographic mass using exact Gaussian–Hermite moments. J Ambient Intell Humaniz Comput 1–9

Ferris LK, Harkes JA, Gilbert B, Winger DG, Golubets K, Akilov O, Satyanarayanan M (2015) Computer-aided classification of melanocytic lesions using dermoscopic images. J Am Acad Dermatol 73(5):769–776

Gambichler T, Jaedicke V, Terras S (2011) Optical coherence tomography in dermatology: technical and clinical aspects. Arch Dermatol Res 303(7):457–473

Goldberger J, Hinton GE, Roweis ST, Salakhutdinov RR (2005) Neighbourhood components analysis. In: Paper presented at the advances in neural information processing systems

Gutman D, Codella NC, Celebi E, Helba B, Marchetti M, Mishra N, Halpern A (2016) Skin lesion analysis toward melanoma detection: a challenge at the international symposium on biomedical imaging (ISBI) 2016, hosted by the international skin imaging collaboration (ISIC). arXiv preprint arXiv:1605.01397

Hendi A, Martinez JC (2011) Atlas of skin cancers: practical guide to diagnosis and treatment. Springer Science & Business Media, New York

Iqbal Z, Khan MA, Sharif M, Shah JH, ur Rehman MH, Javed K (2018) An automated detection and classification of citrus plant diseases using image processing techniques: a review. Comput Electron Agric 153:12–32

Johr RH (2002) Dermoscopy: alternative melanocytic algorithms—the ABCD rule of dermatoscopy, menzies scoring method, and 7-point checklist. Clin Dermatol 20(3):240–247

Kaur M, Kaur J, Kaur J (2011) Survey of contrast enhancement techniques based on histogram equalization. IJACSA Int J Adv Comput Sci Appl 2(7):1–173

Kawahara J, BenTaieb A, Hamarneh G (2016) Deep features to classify skin lesions. Paper presented at the biomedical imaging (ISBI), 2016 IEEE 13th international symposium on

Kawahara J, Daneshvar S, Argenziano G, Hamarneh G (2018) 7-Point checklist and skin lesion classification using multi-task multimodal neural nets. IEEE J Biomed Health Inform

Khalid S, Khalil T, Nasreen S (2014) A survey of feature selection and feature extraction techniques in machine learning. In: Paper presented at the science and information conference (SAI), 2014

Khan MA, Sharif M, Javed MY, Akram T, Yasmin M, Saba T (2017) License number plate recognition system using entropy-based features selection approach with SVM. IET Image Process 12:200–209

Khan MA, Akram T, Sharif M, Shahzad A, Aurangzeb K, Alhussein M, Altamrah A (2018a) An implementation of normal distribution based segmentation and entropy controlled features selection for skin lesion detection and classification. BMC Cancer 18(1):638

Khan MA, Akram T, Sharif M, Javed MY, Muhammad N, Yasmin M (2018b) An implementation of optimized framework for action classification using multilayers neural network on selected fused features. Pattern Anal Appl. https://doi.org/10.1007/s10044-018-0688-1

Kushwaha N, Pant M (2018) Fuzzy magnetic optimization clustering algorithm with its application to health care. J Ambient Intell Humaniz Comput 1–10

Li J, Liu L, Zhou M, Yang J-J, Chen S, Liu H, Tan F (2018) Feature selection and prediction of small-for-gestational-age infants. J Ambient Intell Humaniz Comput. https://doi.org/10.1007/s12652-018-0892-2

Liaqat A, Khan MA, Shah JH, Sharif M, Yasmin M, Fernandes SL (2018) Automated ulcer and bleeding classification from wce images using multiple features fusion and selection. J Mech Med Biol 18(4):1850038

Liu Y, Zheng YF (2005) One-against-all multi-class SVM classification using reliability measures. In: Paper presented at the Neural Networks, 2005. IJCNN'05. Proceedings. 2005 IEEE international joint conference on

Lopez AR, Giro-i-Nieto X, Burdick J, Marques O (2017) Skin lesion classification from dermoscopic images using deep learning techniques. In: Paper presented at the biomedical engineering (BioMed), 2017 13th IASTED international conference on

Machado M, Pereira J, Fonseca-Pinto R (2015) Classification of reticular pattern and streaks in dermoscopic images based on texture analysis. J Med Imaging 2(4):044503

Majtner T, Yildirim-Yayilgan S, Hardeberg JY (2016) Combining deep learning and hand-crafted features for skin lesion classification. In: Paper presented at the image processing theory tools and applications (IPTA), 2016 6th international conference on

Monisha M, Suresh A, Bapu BT, Rashmi M (2018) Classification of malignant melanoma and benign skin lesion by using back propagation neural network and ABCD rule. Cluster Comput 1–11

Nasir M, Attique Khan M, Sharif M, Lali IU, Saba T, Iqbal T (2018) An improved strategy for skin lesion detection and classification using uniform segmentation and feature selection based approach. Microsc Res Tech 81(6):528–543

Okuboyejo DA, Olugbara OO, Odunaike SA (2013) Automating skin disease diagnosis using image classification. In: Paper presented at the proceedings of the world congress on engineering and computer science

Oliveira RB, Papa JP, Pereira AS, Tavares JMR (2018) Computational methods for pigmented skin lesion classification in images: review and future trends. Neural Comput Appl 29(3):613–636

Pennisi A, Bloisi DD, Nardi D, Giampetruzzi AR, Mondino C, Facchiano A (2016) Skin lesion image segmentation using Delaunay Triangulation for melanoma detection. Comput Med Imaging Graph 52:89–103

Permuter H, Francos J, Jermyn I (2006) A study of Gaussian mixture models of color and texture features for image classification and segmentation. Pattern Recogn 39(4):695–706

Prabukumar M, Agilandeeswari L, Ganesan K (2017) An intelligent lung cancer diagnosis system using cuckoo search optimization and support vector machine classifier. J Ambient Intell Humaniz Comput. https://doi.org/10.1007/s12652-017-0655-5

Premaladha J, Ravichandran K (2016) Novel approaches for diagnosing melanoma skin lesions through supervised and deep learning algorithms. J Med Syst 40(4):96

Qin C, Song S, Huang G, Zhu L (2015) Unsupervised neighborhood component analysis for clustering. Neurocomputing 168:609–617

Raja NSM, Fernandes S, Dey N, Satapathy SC, Rajinikanth V (2018) Contrast enhanced medical MRI evaluation using Tsallis entropy and region growing segmentation. J Ambient Intell Humaniz Comput. https://doi.org/10.1007/s12652-018-0854-8

Ravindraiah R (2012) Quality improvement for analysis of leukemia images through contrast stretch methods. Proc Eng 30:475–481

Raza M, Sharif M, Yasmin M, Khan MA, Saba T, Fernandes SL (2018) Appearance based pedestrians' gender recognition by employing stacked auto encoders in deep learning. Future Gener Comput Syst 88:28–39

Read RL, Madronio CM, Cust AE, Goumas C, Watts CG, Menzies S, Morton RL (2018) Follow-up recommendations after diagnosis of primary cutaneous melanoma: a population-based study in New South Wales, Australia. Ann Surg Oncol 25(3):617–625

Shah JH, Chen Z, Sharif M, Yasmin M, Fernandes SL (2017a) A novel biomechanics-based approach for person re-identification by generating dense color sift salience features. J Mech Med Biol 17(07):1740011

Shah JH, Sharif M, Yasmin M, Fernandes SL (2017b) Facial expressions classification and false label reduction using LDA and threefold SVM. Pattern Recognit Lett. https://doi.org/10.1016/j.patrec.2017.06.021

Sharif M, Khan MA, Akram T, Javed MY, Saba T, Rehman A (2017) A framework of human detection and action recognition based on uniform segmentation and combination of Euclidean distance and joint entropy-based features selection. EURASIP J Image Video Process 2017(1):89

Sharif M, Khan MA, Faisal M, Yasmin M, Fernandes SL (2018a) A framework for offline signature verification system: best features selection approach. Pattern Recognit Lett. https://doi.org/10.1016/j.patrec.2018.01.021

Sharif M, Khan MA, Iqbal Z, Azam MF, Lali MIU, Javed MY (2018b) Detection and classification of citrus diseases in agriculture based on optimized weighted segmentation and feature selection. Comput Electron Agric 150:220–234

Shereena V, David JM (2014) Content based image retrieval: classification using neural networks. Int J Multimedia Appl 6(5):31

Siegel RL, Miller KD, Jemal A (2018) Cancer statistics, 2018. CA Cancer J Clin 68(1):7–30

Sng J, Koh D, Siong WC, Choo TB (2009) Skin cancer trends among Asians living in Singapore from 1968 to 2006. J Am Acad Dermatol 61(3):426–432

Stoecker WV, Wronkiewiecz M, Chowdhury R, Stanley RJ, Xu J, Bangert A, Oliviero M (2011) Detection of granularity in dermoscopy images of malignant melanoma using color and texture features. Comput Med Imaging Graph 35(2):144–147

Uddin MZ, Hassan MM, Almogren A, Zuair M, Fortino G, Torresen J (2017) A facial expression recognition system using robust face features from depth videos and deep learning. Comput Electr Eng 63:114–125

Waheed Z, Waheed A, Zafar M, Riaz F (2017) An efficient machine learning approach for the detection of melanoma using dermoscopic images. In: International conference on paper presented at the communication, computing and systems D (C-CODE)

Wu Y, Liu B, Wu W, Lin Y, Yang C, Wang M (2018) Grading glioma by radiomics with feature selection based on mutual information. J Ambient Intell Humaniz Comput. DOI: 10.1007/s12652-018-0883-3

Yang W, Wang K, Zuo W (2012) Neighborhood component feature selection for high-dimensional data. JCP 7(1):161–168

Yu L, Chen H, Dou Q, Qin J, Heng P-A (2017) Automated melanoma recognition in dermoscopy images via very deep residual networks. IEEE Trans Med Imaging 36(4):994–1004

Zhang Q, Lin J, Tao Y, Li W, Shi Y (2017) Salient object detection via color and texture cues. Neurocomputing 243:35–48

Zhu W, Liang S, Wei Y, Sun J (2014) Saliency optimization from robust background detection. In: Paper presented at the proceedings of the IEEE conference on computer vision and pattern recognition

Publisher's Note Springer Nature remains neutral with regard to jurisdictional claims in published maps and institutional affiliations.